Proceedings of HT2007
2007 ASME-JSME Thermal Engineering Summer Heat Transfer Conference
July 8-12, 2007, Vancouver, British Columbia, CANADA

HT2007-32219

VALIDATION OF A GENERAL HEAT TRANSFER CORRELATION FOR NON-BOILING TWO-PHASE FLOW WITH DIFFERENT FLOW PATTERNS AND PIPE INCLINATION ANGLES

Clement C. Tang and Afshin J. Ghajar
School of Mechanical and Aerospace Engineering
Oklahoma State University,
Stillwater, OK 74078, USA
E-mail: ghajar@ceat.okstate.edu

ABSTRACT

A general heat transfer correlation for non-boiling gas-liquid two-phase flow with different flow patterns and inclination angles was developed. To verify the correlation, local heat transfer coefficients and flow parameters were measured for air-water flow in a pipe for the horizontal and slightly upward inclined (2°, 5°, and 7°) positions, and all the flow patterns in the entire flow map. The test section was a 27.9 mm stainless steel pipe with a length to diameter ratio of 95. A total of 763 data points were collected for horizontal and slightly upward inclined positions by carefully coordinating the liquid and gas superficial Reynolds number combinations. The heat transfer data were collected under a uniform wall heat flux boundary condition ranging from about 1800 to 10900 W/m^2. The superficial Reynolds numbers ranged from about 740 to 26000 for water and from about 560 to 48000 for air. The general heat transfer correlation was validated with the 763 data points that were experimentally collected. The validation confirmed the robustness of the general two-phase heat transfer correlation to adequately predict heat transfer data for various flow patterns and inclination angles. The accuracy of the correlation to correlate the experimental data was further explored by applying various available void fraction correlations. The performance of the correlation when applied with the different void fraction correlations were compared and appropriate recommendations are made.

INTRODUCTION

Gas-liquid two-phase flow in pipes is commonly observed in many industrial applications, such as oil wells and pipelines, solar collectors, chemical reactors, and nuclear reactors, and its hydrodynamic and thermal conditions are dependent upon the interaction between the two phases. However, due to the complex nature of the two-phase gas-liquid flow, the accessible heat transfer data and applicable correlations for non-boiling two-phase flow in horizontal and inclined pipes covering various flow patterns and inclined positions are limited in the literature.

Most of the available heat transfer correlations are often limited by specific flow pattern or flow orientation. A comprehensive discussion of the available experimental data and heat transfer correlations for forced convective heat transfer during gas-liquid two-phase flow in vertical and horizontal pipes, including flow patterns and fluid combinations is provided by Kim et al. (1999). However, due to the complex nature of the two-phase gas-liquid flow, no systematic investigation has been conducted to document the influence of flow pattern and inclination angle on the two-phase heat transfer. The only available information on the effect of inclination in the literature is from Hetsroni et al. (1998), and their study was qualitative in nature and limited to slug flow. Their experimental work measured the local heat transfer, using infrared thermography, as a function of slug frequency, slug length and height, inclination angle, and Froude number. Inclination angles were limited to 2° and 5°. They concluded that there was a drastic increase in heat transfer with only slight increases in inclination angle. The authors provided no quantitative information to support the observed increase in the heat transfer. Later, Trimble et al. (2002) quantitatively investigated the effect of inclination on heat transfer in slug flow. In their experimental study, the 2° and 5° data showed an average increase over the horizontal position of about 10% and 20%, respectively. However, their investigation was limited to only one flow pattern (slug flow) and was exploratory in nature and was not conducted systematically.

The objectives of this study were to extend the knowledge base by gathering quality non-boiling, two-phase, two-component heat transfer data in the horizontal and inclined

positions with various flow patterns, and analyze their behavior and extend the capability of a general overall heat transfer coefficient correlation which was developed by our research team, see Ghajar and Kim (2005), and Kim and Ghajar (2006). In order to achieve this goal, the nature of the heat transfer in air-water two-phase flow was investigated by comparing the two-phase heat transfer data that were obtained by systematically varying the air or water flow rates (flow pattern) and the pipe inclination angle.

NOMENCLATURE

C	constant coefficient in Eqs. (1) and (6), dimensionless
D	inside diameter of a circular tube, m
F_P	flow pattern factor, Eq. (3), dimensionless
F_S	shape factor, Eq. (4), dimensionless
g	acceleration due to gravity, m/s^2
h	heat transfer coefficient, W/m^2·K
h_G	heat transfer coefficient as if gas alone were flowing, W/m^2·K
h_L	heat transfer coefficient as if liquid alone were flowing, W/m^2·K
h_{TP}	overall mean two-phase heat transfer coefficient, Eqs. (1) and (6), W/m^2·K
I	inclination factor, Eq. (5), dimensionless
K	slip ratio, dimensionless
k	thermal conductivity, W/m·K
L	length of heat transfer test section, m
m	constant exponent value on the quality ratio term in Eqs. (1) and (6), dimensionless
$\dot{m}$	mass flow rate, kg/s or kg/min
n	constant exponent value on the void fraction ratio term in Eqs. (1) and (6), dimensionless
Pr	Prandtl number, dimensionless
p	constant exponent value on the Prandtl number ratio term in Eqs. (1) and (6), dimensionless
q	constant exponent value on the viscosity ratio term in Eqs. (1) and (6), dimensionless
$\dot{q}''$	heat flux, W/m^2
Re	Reynolds number, dimensionless
Re_L	liquid in-situ Reynolds number, Eq. (7), dimensionless
r	constant exponent value on the inclination factor in Eq. (6), dimensionless
S_L	wetted-perimeter, m
T	temperature, °C
u	axial velocity, m/s
u_{GM}	drift velocity, m/s
x	quality or dryness fraction, dimensionless

Greek Symbols

α	void fraction, dimensionless
μ	dynamic viscosity, Pa-s
θ	inclination angle of a pipe to the horizontal, rad.
ρ	density, kg/m^3
σ	surface tension, N/m

Superscript

$\bar{}$	local mean
~	non-dimensionalized

Subscripts

atm	atmosphere
b	evaluated at bulk temperature
CAL	calculated
EXP	experimental
eq	equilibrium state
eff	effective
G	gas phase
k	index of thermocouple station in test section
L	liquid phase
m	mixture
SG	superficial gas
SL	superficial liquid
sys	system
TP	two-phase
w	evaluated at wall temperature

DEVELOPMENT OF HEAT TRANSFER CORRELATION

In order to predict the heat transfer coefficient in two-phase flow regardless of flow pattern and inclination angle, a new correlation is developed based on the work of Kim et al. (2000). In their work they assumed that the total gas-liquid two-phase heat transfer is the sum of the individual single-phase heat transfers of the gas and liquid, weighted by the volume of each phase present as shown in Eq. (1).

$$h_{TP} = (1-\alpha)\,h_L + \alpha\,h_G = (1-\alpha)\,h_L\left[1 + C\left\{\left(\frac{x}{1-x}\right)^m\left(\frac{\alpha}{1-\alpha}\right)^n\left(\frac{Pr_G}{Pr_L}\right)^p\left(\frac{\mu_G}{\mu_L}\right)^q\right\}\right] \quad (1)$$

Kim et al. (2000) correlation, Eq. (1), has been successfully applied to the experimental data taken in our laboratory [Kim and Ghajar (2002), Ghajar et al. (2004a, b, c), and Ghajar (2005)]. However, the weighting factor (void fraction) used in our correlation does not fully account for the effect of different flow patterns and inclination angles on the two-phase heat transfer data. In the past we had to use different set of constants for different flow patterns (Kim and Ghajar, 2002) and inclination angles (Ghajar et al., 2004a, c). Therefore, in order to handle the effect of various flow patterns and inclination angles on the two-phase heat transfer data with only one correlation, Ghajar and Kim (2005) introduced the flow pattern factor (F_P) and the inclination factor (I).

The void fraction (α) which is the volume fraction of the gas-phase in the tube cross-sectional area, does not reflect the actual wetted-perimeter (S_L) in the tube with respect to the

corresponding flow pattern. For instance, the void fraction and the non-dimensionalized wetted-perimeter of a plug flow both approach unity, but in the case of an annular flow the void fraction is near zero and the wetted-perimeter is near unity. However, the estimation of the actual wetted-perimeter is very difficult due to the continuous interaction of the two phases in the tube. Therefore, instead of estimating the actual wetted-perimeter, modeling the effective wetted-perimeter is a more practical approach. In our model we have ignored the influence of the surface tension and the contact angle of each phase on the effective wetted-perimeter.

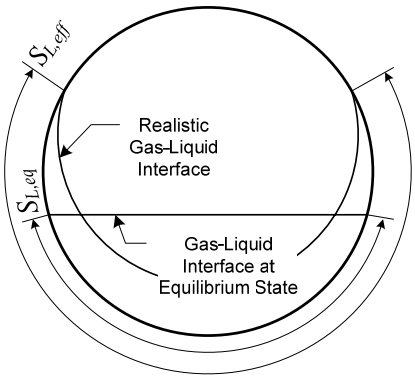

Figure 1: Gas-liquid interfaces and wetted-perimeters

The wetted-perimeter at the equilibrium state, which can be calculated from the void fraction is

$$\widetilde{S}_{L,eq}^{2} = \left(\frac{S_{L,eq}}{\pi D} \right)^{2} = 1 - \alpha \tag{2}$$

However, as shown in Fig. 1, the shape of the gas-liquid interface at the equilibrium state based on the void fraction, α, is far different from the one for the realistic case. As mentioned before, it can also be noticed from Eqs. (1) and (2) that the two-phase heat transfer correlation weighted by the void fraction is not capable of distinguishing the differences between the different flow patterns. Therefore, in order to capture the realistic shape of the gas-liquid interface, the flow pattern factor (F_P), an effective wetted-perimeter relation, which is a modified version of the equilibrium wetted-perimeter, Eq. (2), is proposed,

$$F_P = \widetilde{S}_{L,eff}^{2} = \left(\frac{S_{L,eff}}{\pi D} \right)^{2} = (1-\alpha) + \alpha F_S^2 \tag{3}$$

For simplicity, the above equation for the effective wetted-perimeter relation ($\widetilde{S}_{L,eff}^{2}$) is referred to as the flow pattern factor (F_P). The term F_S appearing in Eq. (3) above is referred to as shape factor which in essence is a modified and normalized Froude number. The shape factor (F_S) is defined as

$$F_S = \frac{2}{\pi} \tan^{-1} \left(\sqrt{\frac{\rho_G \left(u_G - u_L\right)^2}{g\, D \left(\rho_L - \rho_G\right) \cos(\theta)}} \right) \tag{4}$$

The shape factor (F_S) is applicable for slip ratios $K\left(= u_G / u_L\right) \geq 1$, which is common in gas-liquid flow, and represents the shape changes of the gas-liquid interface by the force acting on the interface due to the relative momentum and gravitational forces.

Due to the density difference between gas and liquid, the liquid phase is much more affected by the orientation of flow (inclination). The detailed discussion of the inclination effect on the two-phase heat transfer is available in Ghajar et al. (2004b) and Ghajar and Tang (2007). In order to account for the effect of inclination, the inclination factor, I, is proposed and defined as

$$I = 1 + \frac{g\, D \left(\rho_L - \rho_G\right) \sin(\theta)}{\rho_L\, u_{SL}^2} \tag{5}$$

where the term $[g\, D \left(\rho_L - \rho_G\right) \sin(\theta)] / [\rho_L\, u_{SL}^2]$ represents the relative force acting on the liquid phase in the flow direction due to the momentum and the gravitational forces.

Now, introduce the two proposed factors for the flow pattern (F_P) and inclination (I) effects into our heat transfer correlation, Eq. (1). Substituting F_P for $\left(1-\alpha\right)$ which is the leading coefficient of h_L and introducing I as an additional power-law term in Eq. (1), the correlation becomes

$$h_{TP} = F_P\, h_L \left\{ 1 + C \left[\left(\frac{x}{1-x} \right)^{m} \left(\frac{1-F_P}{F_P} \right)^{n} \left(\frac{Pr_G}{Pr_L} \right)^{p} \left(\frac{\mu_G}{\mu_L} \right)^{q} (I)^{r} \right] \right\} \tag{6}$$

where h_L comes from the Sieder and Tate (1936) correlation for turbulent flow:

$$h_L = 0.027\, Re_L^{4/5}\, Pr_L^{1/3} \left(\frac{k_L}{D} \right) \left(\frac{\mu_b}{\mu_w} \right)_L^{0.14} \tag{7}$$

For the Reynolds number needed in the h_L calculation, the following relationship is used to evaluate the in-situ Reynolds number (liquid phase) rather than the superficial Reynolds number (Re_{SL}) as commonly used in the correlations available in the literature (see Kim et al., 1999):

$$Re_L = \left(\frac{\rho u D}{\mu} \right)_L = \frac{4\dot{m}_L}{\pi \sqrt{1-\alpha}\, \mu_L D} \tag{8}$$

Since the flow pattern factor (F_P) and the in-situ Reynolds number (Re_L) require the input of void fraction, questions arise as to how well the general two-phase heat transfer correlation, Eq. (6), performs with different void fraction correlations. In this study, six different void fraction correlations were applied to Eqs. (3) and (8). The performance of the general two-phase heat transfer correlation, Eq. (6), was then validated with experimental data from Ghajar and Tang (2007). The first void fraction correlation was provided by Lockhart and Martinelli (1949):

$$\alpha = \left[1 + 0.28 \left(\frac{1-x}{x} \right)^{0.64} \left(\frac{\rho_G}{\rho_L} \right)^{0.36} \left(\frac{\mu_L}{\mu_G} \right)^{0.07} \right]^{-1} \tag{9}$$

The second void fraction correlation was that of Chisholm (1973):

$$\alpha = \left[1 + \left(\frac{\rho_L}{\rho_m} \right)^{1/2} \left(\frac{1-x}{x} \right) \left(\frac{\rho_G}{\rho_L} \right) \right]^{-1} \tag{10}$$

where $1/\rho_m = (1-x)/\rho_L + x/\rho_G$. The third void fraction correlation was developed by Spedding and Chen (1984):

$$\alpha = \left[1 + 2.22 \left(\frac{1-x}{x} \right)^{0.65} \left(\frac{\rho_G}{\rho_L} \right)^{0.65} \right]^{-1} \tag{11}$$

The void fraction correlations given in Eqs. (9) to (11) are considered slip ratio correlations, as they have expressions that resembled the slip ratio.

The fourth void fraction equation was provided by Rouhani and Axelsson (1970):

$$\alpha = \frac{x}{\rho_G} \left[C_0 \left(\frac{x}{\rho_G} + \frac{1-x}{\rho_L} \right) + \left(\frac{u_{GM}}{G} \right) \right]^{-1} \tag{12}$$

where the drift velocity is $u_{GM} = 1.18 \left[g\sigma(\rho_L - \rho_G)/\rho_L^2 \right]^{0.25}$ and $C_0 = 1 + 0.2(1-x)$. The fifth void fraction correlation was developed by Dix as reported in Coddington and Macian (2002):

$$\alpha = u_{SG} \left\{ u_{SG} \left[1 + \left(\frac{u_{SL}}{u_{SG}} \right)^{(\rho_G/\rho_L)^{0.1}} \right] + 2.9 \left[\frac{g\sigma(\rho_L - \rho_G)}{\rho_G^2} \right]^{0.25} \right\}^{-1} \tag{13}$$

Finally, the last void fraction correlation considered in this study was provided by Woldesemayat and Ghajar (2007):

$$\alpha = u_{SG} \left\{ u_{SG} \left[1 + \left(\frac{u_{SL}}{u_{SG}} \right)^{(\rho_G/\rho_L)^{0.1}} \right] + 2.9 C_1 \left[\frac{C_2 g\sigma(\rho_L - \rho_G)}{\rho_G^2} \right]^{0.25} \right\}^{-1} \tag{14}$$

where $C_1 = (1.22 + 1.22\sin\theta)^{P_{atm}/P_{sys}}$ and $C_2 = D(1+\cos\theta)$. The void fraction correlations given in Eqs. (12) to (14) are considered drift flux correlations.

EXPERIMENTAL SETUP AND DATA REDUCTION

A schematic diagram of the overall experimental setup for heat transfer measurements is shown in Fig. 2. The test section is a 27.9 mm I.D. straight standard stainless steel schedule 10S pipe with a length to diameter ratio of 95. The setup rests atop a 9 m long aluminum I-beam that is supported by a pivoting foot and a stationary foot that incorporates a small electric screw jack.

In order to apply uniform wall heat flux boundary condition to the test section, copper plates were silver soldered to the inlet and exit of the test section. The uniform wall heat flux boundary condition was maintained by a Lincoln SA-750 welder for Re_{SL} > 2000 and a Miller Maxtron 450 DC welder for Re_{SL} < 2000. The Lincoln SA-750 welder has the capability of supplying 300 A to 750 A of current, while the Miller Maxtron 450 DC welder is capable of supplying 5 A to 450 A of current. The entire length of the test section was wrapped using fiberglass pipe wrap insulation, followed by a thin polymer vapor seal to prevent moisture penetration.

The calming section (clear polycarbonate pipe with 25.4 mm I.D. and L/D = 88) served as a flow developing and turbulence reduction device, and flow pattern observation section. One end of the calming section is connected to the test section with an acrylic flange and the other end of the calming section is connected to the gas-liquid mixer. For the horizontal flow measurements, the test section, and the observation section (refer to Fig. 2) were carefully leveled to eliminate the effect of inclination on these measurements.

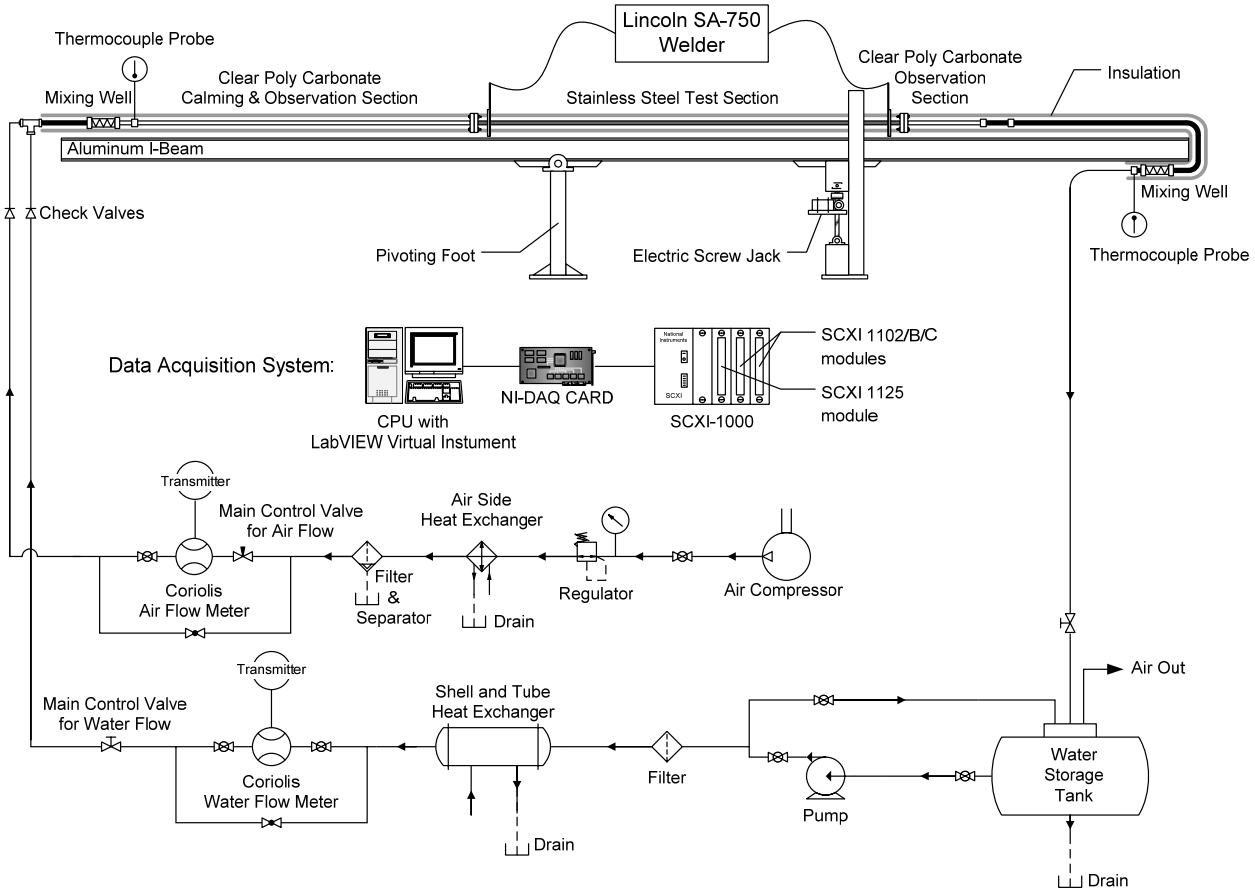

Figure 2: Schematic of experimental setup

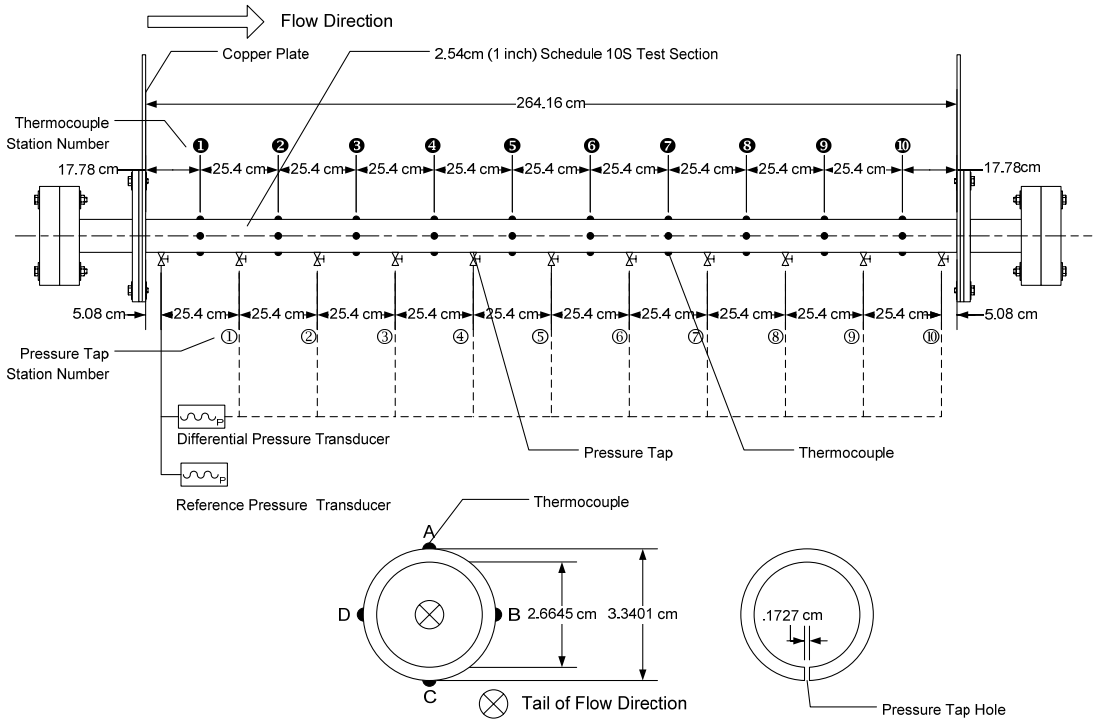

Figure 3: Test section

T-type thermocouple wires were cemented with Omegabond 101, an epoxy adhesive with high thermal conductivity and electrical resistivity, to the outside wall of the stainless steel test section as shown in Fig. 3. OMEGA EXPP-T-20-TWSH extension wires were used for relay to the data acquisition system. Thermocouples were placed on the outer surface of the pipe wall at uniform intervals of 254 mm from the entrance to the exit of the test section. There were 10 thermocouple stations in the test section. All stations had four thermocouples, and they were labeled looking at the tail of the fluid flow with peripheral location 'A' being at the top of the pipe, 'B' being 90° in the clockwise direction, 'C' at the bottom of the pipe, and 'D' being 90° from the bottom in the clockwise sense (refer to Fig. 3). All the thermocouples were monitored with a National Instruments data acquisition system. The experimental data were averaged over a user chosen length of time (typically 20 samples/channel with a sampling rate of 400 scans/sec) before the heat transfer measurements were actually recorded. The average system stabilization time period was from 30 to 60 min after the system attained steady state. The inlet liquid and gas temperatures and the exit bulk temperature were measured by Omega TMQSS-125U-6 thermocouple probes. The thermocouple probe for the exit bulk temperature was placed after the mixing well. Calibration of thermocouples and thermocouple probes showed that they were accurate within ±0.5°C. The operating pressures inside the experimental setup were monitored with a pressure transducer.

To ensure a uniform fluid bulk temperature at the inlet and exit of the test section, a mixing well was utilized. An alternating polypropylene baffle type static mixer for both gas and liquid phases was used. This mixer provided an overlapping baffled passage forcing the fluid to encounter flow reversal and swirling regions. The mixing well at the exit of the test section was placed below the clear polycarbonate observation section (after the test section), and before the liquid storage tank (refer to Fig. 2). Since the cross-sectional flow passage of the mixing section was substantially smaller than the test section, it had the potential of increasing the system back-pressure. Thus, in order to reduce the potential back-pressure problem, which might affect the flow pattern inside of the test section, the mixing well was placed below and after the test section and the clear observation sections. The outlet bulk temperature was measured immediately after the mixing well.

The fluids used in the test loop are air and water. The water is distilled and stored in a 55-gallon cylindrical polyethylene tank. A Bell & Gosset series 1535 coupled centrifugal pump was used to pump the water through an Aqua-Pure AP12T water filter. An ITT Standard model BCF 4063 one shell and two-tube pass heat exchanger removes the pump heat and the heat added during the test to maintain a constant inlet water temperature. From the heat exchanger, the water passes through a Micro Motion Coriolis flow meter (model CMF100) connected to a digital Field-Mount Transmitter (model RFT9739) that conditions the flow information for the data acquisition system. Once the water passes through the Coriolis flow meter it then passes through a 25.4 mm, twelve-turn gate valve that regulates the amount of flow that entered the test section. From this point, the water travels through a 25.4 mm flexible hose, through a one-way check valve, and into the test section. Air is supplied via an Ingersoll-Rand T30 (model 2545) industrial air compressor mounted outside the laboratory and isolated to reduce vibration onto the laboratory floor. The air passes through a copper coil submerged in a vessel of water to lower the temperature of the air to room temperature. The air is then filtered and condensate removed in a coalescing filter. The air flow is measured by a Micro Motion Coriolis flow meter (model CMF025) connected to a digital Field-Mount Transmitter (model RFT9739) and regulated by a needle valve. Air is delivered to the test section by flexible tubing. The water and air mixture is returned to the reservoir where it is separated and the water recycled.

The heat transfer measurements at uniform wall heat flux boundary condition were carried out by measuring the local outside wall temperatures at 10 stations along the axis of the pipe and the inlet and outlet bulk temperatures in addition to other measurements such as the flow rates of gas and liquid, room temperature, voltage drop across the test section, and current carried by the test section. The peripheral heat transfer coefficient (local average) was calculated based on the knowledge of the pipe inside wall surface temperature and inside wall heat flux obtained from a data reduction program developed exclusively for this type of experiments (Ghajar and Kim, 2006). The local average peripheral values for inside wall temperature, inside wall heat flux, and heat transfer coefficient were then obtained by averaging all the appropriate individual local peripheral values at each axial location.

The variation in the circumferential wall temperature distribution, which is typical for two-phase gas-liquid flow in horizontal pipes, leads to different heat transfer coefficients depending on which circumferential wall temperature was selected for the calculations. In two-phase heat transfer experiments, in order to overcome the unbalanced circumferential heat transfer coefficients and to get a representative heat transfer coefficient for a test run, Eq. (15) was used to calculate an overall two-phase heat transfer coefficient ($h_{TP_{EXP}}$) for each test run.

$$h_{TP_{EXP}} = \frac{1}{L}\int \overline{h}\, dz = \frac{1}{L}\sum_{k=1}^{N_{ST}} \overline{h}_k\, \Delta z_k = \frac{1}{L}\sum_{k=1}^{N_{ST}} \left(\frac{\overline{\dot{q}''}}{\overline{T}_w - T_b} \right)_k \Delta z_k \quad (15)$$

where L is the length of the test section, $\overline{h}$, $\overline{\dot{q}''}$, $\overline{T}_w$, T_b are the local mean heat transfer coefficient, the local mean heat flux, the local mean wall temperature, and the bulk temperature at a thermocouple station, respectively; k is the index of the thermocouple stations, N_{ST} is the number of the thermocouple stations, z is the axial coordinate, and Δz is the element length of each thermocouple station.

The data reduction program used a finite-difference formulation to determine the inside wall temperature and the inside wall heat flux from measurements of the outside wall temperature, the heat generation within the pipe wall, and the thermophysical properties of the pipe material (electrical resistivity and thermal conductivity). In these calculations, axial conduction was assumed negligible, but peripheral and radial conduction of heat in the pipe wall were included. In addition, the bulk fluid temperature was assumed to increase linearly from the inlet to the outlet.

A National Instruments data acquisition system was used to record and store the data measured during these experiments. The data acquisition system is housed in an AC powered four-slot SCXI 1000 Chassis that serves as a low noise environment for signal conditioning. Three NI SCXI control modules are housed inside the chassis. There are two SCXI 1102/B/C modules and one SCXI 1125 module. From these three modules, input signals for all 40 thermocouples, the two thermocouple probes, voltmeter, and flow meters are gathered and recorded. The computer interface used to record the data is a LabVIEW Virtual Instrument (VI) program written for this specific application.

The reliability of the flow circulation system and of the experimental procedures was checked by making several single-phase calibration runs with distilled water. The single-phase heat transfer experimental data were checked against the well established single-phase heat transfer correlations (Kim and Ghajar, 2002) in the Reynolds number range from 3000 to 30,000. In most instances, the majority of the experimental results were well within ±10% of the predicted results (Kim and Ghajar, 2002; Durant, 2003). In addition to the single-phase calibration runs, a series of two-phase, air-water, slug flow tests were also performed for comparison against the two-phase experimental slug flow data of Kim and Ghajar (2002), and Trimble et al. (2002). The results of these comparisons, for majority of the cases were also well within the ±10% deviation range.

The uncertainty analysis of the overall experimental procedures using the method of Kline and McClintock (1953) showed that there is a maximum of 11.5% uncertainty for heat transfer coefficient calculations. Experiments under the same conditions were conducted periodically to ensure the repeatability of the results. The maximum difference between the duplicated experimental runs was within ±10%. More details of experimental setup and data reduction procedures can be found from Durant (2003).

The heat transfer data obtained with the present experimental setup were measured under a uniform wall heat flux boundary condition that ranged from 1860 W/m^2 to 10900 W/m^2 and the resulting two-phase heat transfer coefficients ($h_{TP_{EXP}}$) ranged from 101 W/m^2·K to 5700 W/m^2·K for horizontal flow. For these experiments, the superficial liquid Reynolds number (Re_{SL}) ranged from 740 to 26100 (water mass flow rates from 0.761 kg/min to 42.5 kg/min) and the superficial gas Reynolds numbers (Re_{SG}) ranged from 560 to 47600 (air mass flow rates from 0.013 kg/min to 1.13 kg/min). The summary of the experimental conditions and measured heat transfer coefficients is tabulated in Table 1. Detailed discussions on the complete experimental results are documented by Ghajar and Tang (2007).

Table 1: Summary of experimental conditions and measured two-phase heat transfer data

	Test section orientation			
	Horizontal	2° inclined	5° inclined	7° inclined
No. of data points	208	184	184	187
Re_{SL} range	740–26100	750–25900	780–25900	770–26000
Re_{SG} range	700–47600	700–47500	590–47500	560–47200
$\dot{q}''$ range [W/m^2]	1860–10800	2820–10800	2900–10800	2600–10900
$h_{TP_{EXP}}$ range [W/m^{2}K]	101–5457	242–5140	286–5507	364–5701

FLOW PATTERNS

The various interpretations accorded to the multitude of flow patterns by different investigators are subjective; and no uniform procedure exists at present for describing and classifying them. In this study, the flow pattern identification for the experimental data was based on the procedures suggested by Taitel and Dukler (1976), and Kim and Ghajar (2002); and visual observations deemed appropriate. All observations for the flow pattern judgments were made at the clear polycarbonate observation sections before and after the stainless steel test section (see Fig. 2). By fixing the water flow rate, flow patterns were observed by varying air flow rates. Flow pattern data were obtained at isothermal condition with the pipe at horizontal position and at 2°, 5°, and 7° inclined positions. These experimental data were plotted and compared using their corresponding values of Re_{SG} and Re_{SL}, and the flow patterns. Representative digital images of each flow pattern were taken using a Nikon D50 digital camera with Nikkor 50mm f/1.8D lens. Figure 4 shows the flow map for horizontal flow with the representative photographs of the various flow patterns. The various flow patterns for horizontal flow depicted in Fig. 4 show the capability of our experimental setup to cover multitude of flow patterns. The shaded regions represent the transition boundaries of the observed flow patterns.

The influence of small inclination angles of 2°, 5°, and 7° on the observed flow patterns is shown in Fig. 5. Table 2 summarizes the number of two-phase heat transfer data points systematically measured for different flow patterns and test section orientation. As shown in Fig. 5, the flow pattern transition boundaries for horizontal flow were found to be quite different from the flow pattern transition boundaries for

inclined flow when slight inclinations of 2°, 5°, and 7° were introduced. The changes in the flow pattern transition boundaries from horizontal to slightly inclined flow are the transition boundaries for stratified flow and slug/wavy flow. When the pipe was inclined from horizontal to slight inclination angles of 2°, 5°, and 7°, the stratified flow region was replaced by slug flow and slug/wavy flow for $Re_{SG} < 4000$ and $4000 < Re_{SG} < 10000$, respectively.

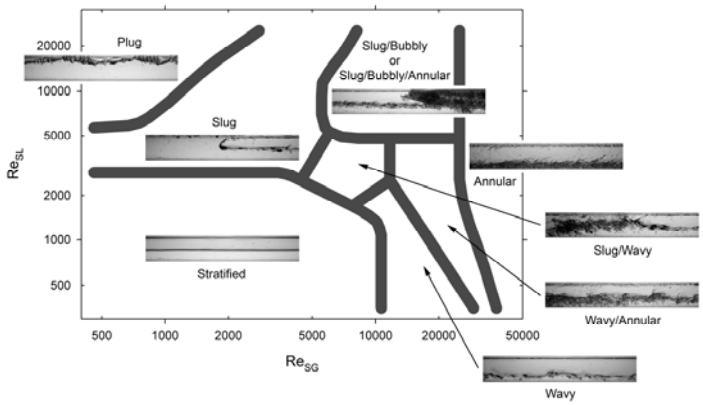

Figure 4: Flow map for horizontal flow with representative photographs of flow patterns

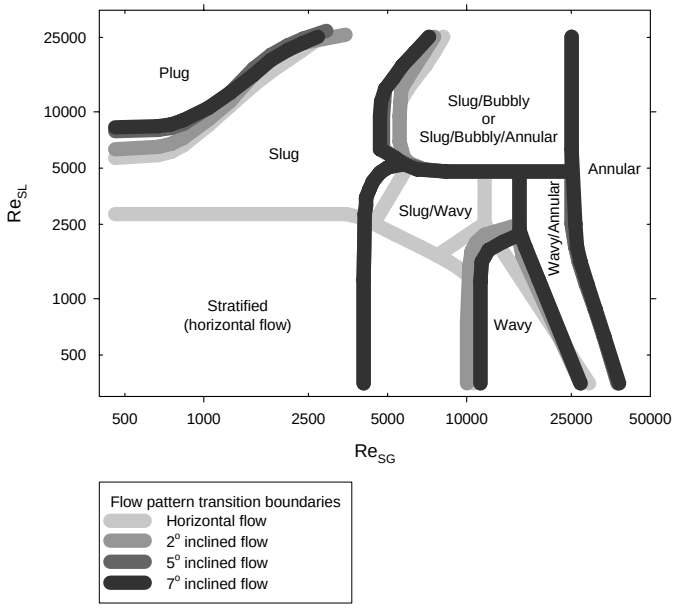

Figure 5: Change of flow pattern transition boundaries as pipe inclined upward from horizontal position

Other shifts in the flow pattern transition boundaries were observed in the plug-to-slug boundary and the slug-to-slug/bubbly boundary. In these two cases, the flow pattern transition boundaries were observed to be shifted slightly to the upper left direction as inclination angles were slightly increased from horizontal to 7°. For slightly inclined flow of 2, 5°, and 7°, there were no drastic changes in the flow pattern transition boundaries. However, it should be mentioned that although the flow patterns were named the same for both horizontal and inclined flow; it does not mean that the flow patterns in the inclined positions have identical characteristics of the comparable flow patterns in the horizontal position. For example, it was observed that the slug flow patterns in the inclined positions of 5° and 7° have reverse flow between slugs due to the gravitational force, which can have a significant effect on the heat transfer.

Table 2: Number of two-phase heat transfer data points measured for different flow patterns and test section orientation

	Test section orientation			
	Horizontal	2° inclined	5° inclined	7° inclined
Stratified	20			
Slug	39	44	43	40
Plug	13	14	11	12
Slug/Wavy	7	15	15	15
Wavy	10	8	10	10
Wavy/Annular	22	11	9	9
Slug/Bubbly/Annular	40	47	50	52
Annular	57	45	46	49

HEAT TRANSFER CORRELATION AND RESULTS

The general heat transfer correlation capable of handling various flow patterns and inclination angles is in the form given by Eq. (6). With the constant and exponents of Eq. (6) set for $C = 0.7$, $m = 0.08$, $n = 0.06$, $p = 0.03$, $q = -0.14$, and $r = 0.65$, Eq. (6) was successfully validated with a total of 408 experimental data points for different flow patterns and inclination angles (Ghajar and Kim, 2005; Kim and Ghajar, 2006; Ghajar et al., 2006).

Since then additional heat transfer data was measured, which brings the complete experimental heat transfer database to a total of 763 data points (Ghajar and Tang, 2007). The additional heat transfer data points were measured for $Re_{SL} < 5000$ with different inclination angles. With the additional experimental data points, it is necessary to adjust the constant and exponents of Eq. (6) to improve its agreement with the experimental data. The adjusted constant and exponents of Eq. (6) are $C = 0.84$, $m = 0.04$, $n = 0.4$, $p = 0.04$, $q = -0.01$, and $r = 0.34$.

By applying the six different void fraction correlations to the general two-phase heat transfer correlation, Eq. (6), the results from the Eq. (6) were compared with the 763 experimental data points. Detailed results of the prediction by the heat transfer correlation, Eq. (6), for each of the six void fraction correlations are summarized in Table 3.

Table 3: Results predicted by the general two-phase heat transfer correlation, Eq. (6), compared with 763 measured data points

Void fraction correlations	Value of C and Exponents (m, n, p, q, r)						Abs. Mean Dev. [%]	Range of Mean Dev. [%]	No. of Data within ±20%	No. of Data within ±30%
	C	m	n	p	q	r				
Lockhart & Martinelli (1949), Eq. (9)	0.84	0.04	0.4	0.04	-0.01	0.34	21.4	-13.6 to 26.6	525 (68.8%)	644 (84.4%)
Chisholm (1973), Eq. (10)							21.1	-16.9 to 31.6	497 (65.1%)	637 (83.5%)
Spedding & Chen (1984), Eq. (11)							20.3	-11.1 to 25.7	572 (75.0%)	653 (85.6%)
Rouhani & Axelsson (1970), Eq. (12)							28.1	-13.8 to 43.1	473 (62.0%)	617 (80.9%)
Dix (Coddington & Macian, 2002), Eq. (13)							28.9	-13.2 to 42.7	490 (64.2%)	606 (79.4%)
Woldesemayat & Ghajar (2007), Eq. (14)							25.8	-14.7 to 43.0	504 (66.1%)	606 (79.4%)

Table 4: Determined constants for each void fraction correlation applied to Eq. (6), and the results predicted by Eq. (6) compared with 763 measured data points

Void fraction correlations	Value of C and Exponents (m, n, p, q, r)						Abs. Mean Dev. [%]	Range of Mean Dev. [%]	No. of Data within ±20%	No. of Data within ±30%
	C	m	n	p	q	r				
Lockhart & Martinelli (1949), Eq. (9)	0.79	0.08	0.41	0.04	-0.01	0.41	20.9	-13.5 to 31.6	529 (69.3%)	653 (85.6%)
Chisholm (1973), Eq. (10)	1	0.05	0.42	0.03	-0.01	0.39	22.5	-11.8 to 34.1	548 (71.8%)	650 (85.2%)
Spedding & Chen (1984), Eq. (11)	0.82	0.08	0.39	0.03	-0.01	0.4	19.7	-10.4 to 31.6	582 (76.3%)	673 (88.2%)
Rouhani & Axelsson (1970), Eq. (12)	0.84	0.04	0.33	0.03	-0.01	0.27	25.6	-14.8 to 38.6	485 (63.6%)	625 (81.9%)
Dix (Coddington & Macian, 2002), Eq. (13)	0.9	0.08	0.4	0.03	-0.01	0.26	27.1	-14.3 to 45.0	504 (66.1%)	615 (80.6%)
Woldesemayat & Ghajar (2007), Eq. (14)	0.91	0.04	0.4	0.03	-0.01	0.29	25.5	-13.3 to 39.0	510 (66.8%)	628 (82.3%)

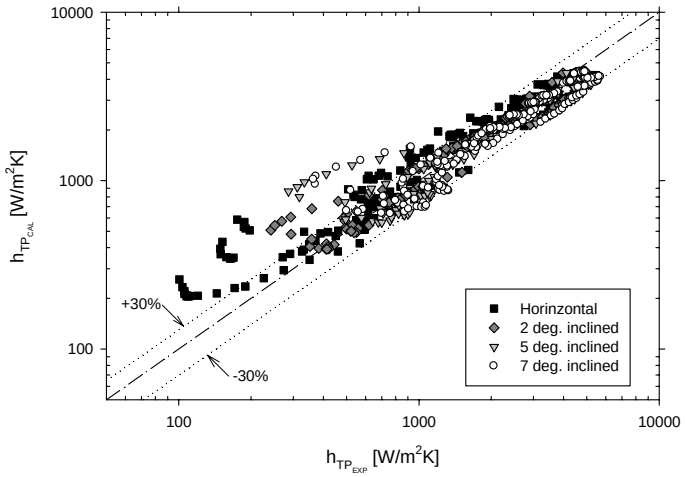

(a) Using Lockhart and Martinelli (1949)

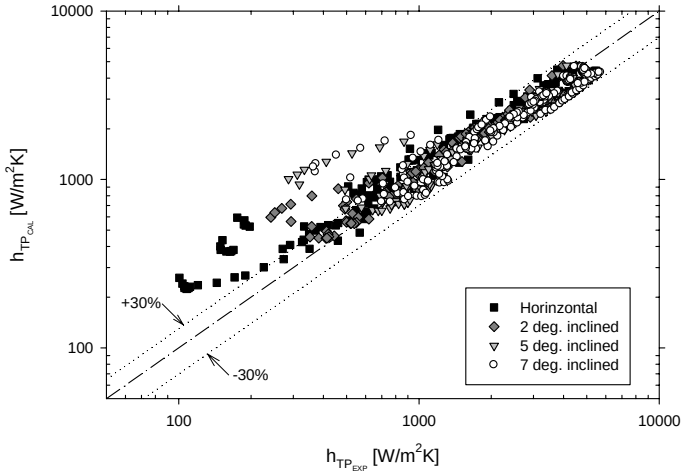

(b) Using Chisholm (1973)

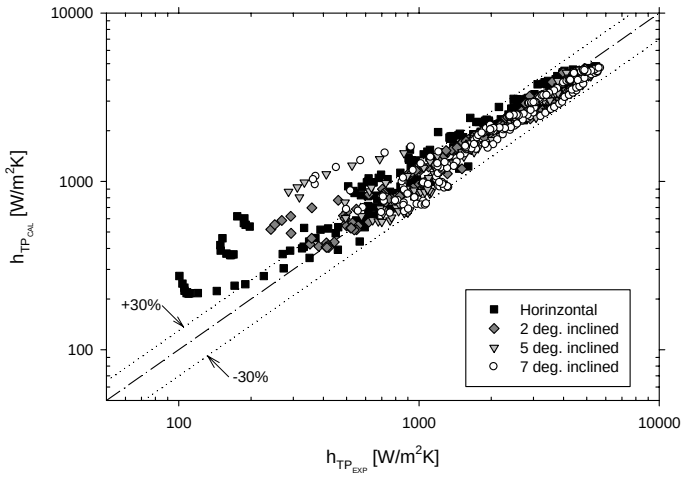

(c) Using Spedding and Chen (1984)

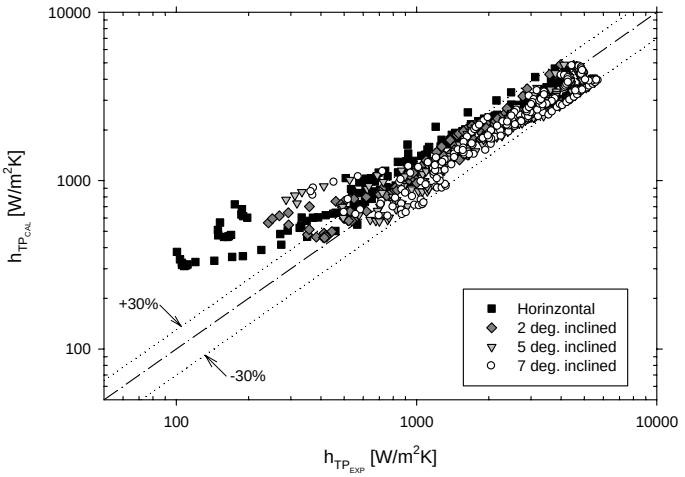

(d) Using Rouhani and Axelsson (1970)

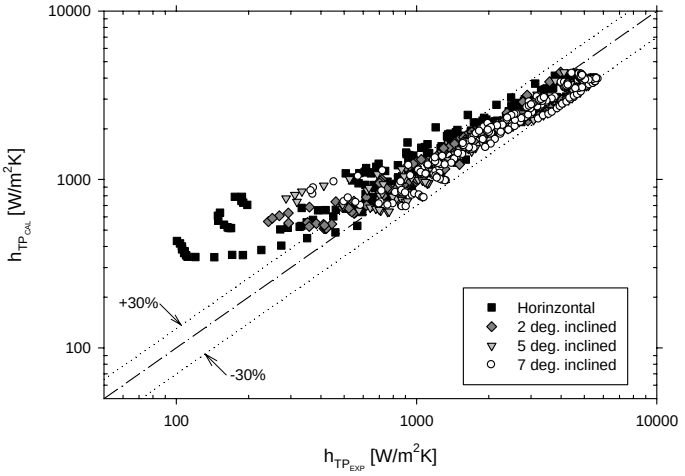

(e) Using Dix (Coddington & Macian, 2002)

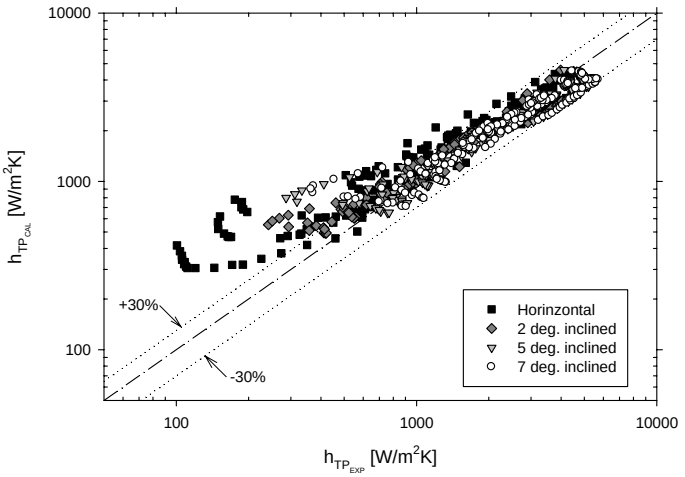

(f) Using Woldesemayat and Ghajar (2007)

Figure 6: Results from Eq. (6) when applied with different void fraction correlations and the appropriate constants and exponents listed in Table 4 are compared with the experimental data

Table 5: Summary of the results predicted by Eq. (6) when applied with the various void fraction correlations and the corresponding constants listed in Table 4 for different inclination angles and superficial liquid Reynolds number ranges

Category of exp. data (No. of data points)	No. of data points predicted by Eq. (6) within ±30% of experimental data					
	Slip ratio correlations			Drift flux correlations		
	Lockhart & Martinelli (1949), Eq. (9)	Chisholm (1973), Eq. (10)	Spedding & Chen (1984), Eq. (11)	Rouhani & Axelsson (1970), Eq. (12)	Dix (Coddington & Macian, 2002), Eq. (13)	Woldesemayat & Ghajar (2007), Eq. (14)
Horizontal (208)	153 (73.6%)	145 (69.7%)	151 (72.6%)	131 (63.0%)	134 (64.4%)	135 (64.9%)
$Re_{SL} < 2000$ (43)	25 (58.1%)	15 (34.9%)	23 (53.5%)	9 (20.9%)	13 (30.2%)	14 (32.6%)
$2000 < Re_{SL} < 10000$ (87)	52 (59.8%)	55 (63.2%)	51 (58.6%)	48 (55.2%)	44 (50.6%)	45 (51.7%)
$Re_{SL} > 10000$ (78)	76 (97.4%)	75 (96.2%)	77 (98.7%)	74 (94.9%)	77 (98.7%)	76 (97.4%)
2° inclined (184)	176 (95.7%)	170 (92.4%)	175 (95.1%)	171 (92.9%)	161 (87.5%)	164 (89.1%)
$Re_{SL} < 2000$ (36)	28 (77.8%)	22 (61.1%)	27 (75.0%)	23 (63.9%)	18 (50.0%)	20 (55.6%)
$2000 < Re_{SL} < 10000$ (72)	72 (100%)	72 (100%)	72 (100%)	72 (100%)	67 (93.1%)	68 (94.4%)
$Re_{SL} > 10000$ (76)	76 (100%)	76 (100%)	76 (100%)	76 (100%)	76 (100%)	76 (100%)
5° inclined (184)	166 (90.2%)	166 (90.2%)	172 (93.5%)	165 (89.7%)	162 (88.0%)	167 (90.8%)
$Re_{SL} < 2000$ (36)	24 (66.7%)	18 (50%)	24 (66.7%)	24 (66.7%)	24 (66.7%)	23 (63.9%)
$2000 < Re_{SL} < 10000$ (72)	72 (100%)	72 (100%)	72 (100%)	72 (100%)	72 (100%)	72 (100%)
$Re_{SL} > 10000$ (76)	70 (92.1%)	76 (100%)	76 (100%)	69 (90.8%)	66 (86.8%)	72 (94.7%)
7° inclined (187)	158 (84.5%)	169 (90.4%)	175 (93.6%)	158 (84.5%)	158 (84.5%)	162 (86.6%)
$Re_{SL} < 2000$ (36)	24 (66.7%)	18 (50%)	25 (69.4%)	25 (69.4%)	26 (72.2%)	25 (69.4%)
$2000 < Re_{SL} < 10000$ (72)	67 (93.1%)	72 (100%)	71 (98.6%)	71 (98.6%)	72 (100%)	72 (100%)
$Re_{SL} > 10000$ (79)	67 (84.8%)	79 (100%)	79 (100%)	62 (78.5%)	60 (75.9%)	65 (82.3%)

The results presented in Table 3 show the general two-phase heat transfer correlation has the robustness that different void fraction correlations can be applied to it. When compared with the experimental data, the general two-phase heat transfer correlation performed reasonably accurate with over 80% of the total data points calculated to be within the ±30% deviation band of the experimental data. Table 3 also shows that the slip ratio void fraction correlations [*i.e.*, Eqs. (9), (10), and (11)] yielded better agreement with the experimental data than the drift flux void fraction correlations [*i.e.*, Eqs. (12), (13), and (14)].

To further improve the results from the general two-phase heat transfer correlation, the constant and exponents in Eq. (6) can be adjusted for each individual void fraction correlations. Table 4 shows the results of Eq. (6) for each of the six void fraction correlations compared with the experimental data. Similarly, Table 4 shows that the slip ratio void fraction correlations yielded better agreement with the experimental data than the drift flux void fraction correlations.

Among the six void fraction correlations applied to Eq. (6), the correlation provided by Spedding and Chen (1984), Eq. (11), yielded the best agreement with the experimental data. Figures 6a to 6f show the capability of the general two-phase heat transfer correlation, Eq. (6), in predicting the experimental data when applied with the six void fraction correlations and the appropriate constants and exponents listed in Table 4.

By comparing Tables 3 and 4, the results from the individually adjusted constants and exponents of Eq. (6) for a given void fraction correlation (see Table 4) showed slight improvement in accuracy but not significant. This shows the robustness of the general two-phase flow heat transfer correlation when applied with various void fraction correlations available in the literature. It should be noted that the constants and exponents listed in Table 4 should be used with the corresponding void fraction correlation, as they were adjusted to give better agreement with the experimental data.

Table 5 summarizes the results predicted by the general two-phase heat transfer correlation, Eq. (6), when applied with the various void fraction correlations and adjusted constants listed in Table 4 for different inclination angles and superficial liquid Reynolds number ranges. Overall, the results listed in Table 5 show that the general two-phase heat transfer correlation is performing more accurately for inclined (2°, 5°, and 7°) flows than horizontal flow regardless of which void fraction correlation was used. For inclined flow, about 85% to 96% of the data points predicted by Eq. (6) is within ±30% of the experimental data points.

Table 5 also shows that the general two-phase heat transfer correlation performed better for higher ranges of superficial liquid Reynolds number. For horizontal flow, about 95% or more of the data were predicted within ±30% for $Re_{SL} > 10000$. For inclined (2°, 5°, and 7°) flows, Eq. (6) when applied with slip ratio void fraction correlations predicted about 85% or more of the data points within ±30% of the experimental data for $Re_{SL} > 2000$.

Tables 3 to 5 and Fig. 6c show that the Spedding and Chen (1984) void fraction correlation, Eq. (11), is the more suitable correlation to be used in the general two-phase heat transfer correlation, Eq. (6); since it resulted with more data points within the ±20% and ±30% bands, and also lower absolute mean deviation and smaller range of mean deviation. Figure 7 shows the comparison of the data calculated by Eq. (6) with the experimental data for inclined (2°, 5°, and 7°) flows at $Re_{SL} > 2000$. The agreement with the experimental data is excellent with all the data predicted within the ±30% band.

Based on the results presented in Table 5, our near future plans are to focus on improving the predictive capabilities of Eq. (6) for horizontal flows with $Re_{SL} < 10000$ and inclined (2°, 5°, and 7°) flows with $Re_{SL} < 2000$. One possibility could be to introduce additional physical parameters in Eq. (6) to better capture the heat transfer mechanisms in these regions.

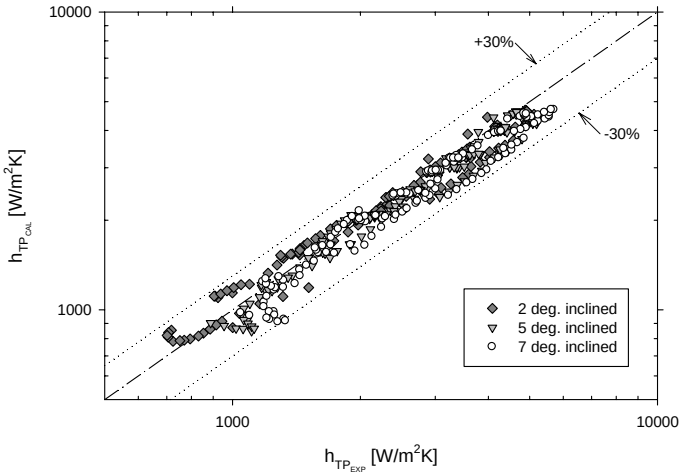

Figure 7: Results from Eq. (6) when applied with Spedding & Chen (1984) for 2°, 5°, and 7° inclined flows at $Re_{SL} > 2000$

CONCLUSIONS

The purpose of this study was to further develop the knowledge and understanding of heat transfer in non-boiling two-phase, two-component flow. For this purpose air-water flow heat transfer experiments were conducted in a circular pipe in the horizontal and slightly upward inclined positions at 2°, 5°, and 7° under uniform wall heat flux boundary condition.

The validation of the general two-phase flow heat transfer correlation, Eq. (6), with 763 experimental data points summarized in Table 1 showed that the correlation is reasonably accurate and has the robustness to handle various flow patterns and pipe inclination angles. Further validation with various void fraction correlations also showed that the general two-phase flow heat transfer correlation can be applied with various void fraction correlations available in the literature. The validation also suggested that the correlation with the constants and exponents listed in Table 4 may be recommended for estimating non-boiling two-phase flow heat

transfer coefficients within the accuracy summarized in Tables 4 and 5 for various flow patterns and pipe inclination angles.

For inclined (2°, 5°, and 7°) flows with superficial Reynolds number greater than 2000, the validation also showed that the Spedding and Chen (1984) void fraction correlation is the more suitable correlation for the general two-phase heat transfer correlation, which resulted with all the data being predicted within ±30% of the experimental data (see Fig. 7). Hence, the general two-phase heat transfer correlation can be very useful for many practical situations, where slight pipe inclination usually exists and the superficial liquid Reynolds numbers are mostly above 2000.

ACKNOWLEDGMENTS

Generous contributions in equipment and software made by Micro Motion and National Instruments are greatly acknowledged.

REFERENCES

Chisholm, D. (1973), Two-Phase Flow in Pipelines and Heat Exchangers, George Godwin, London and New York in association with the Institution of Chemical Engineers, New York.

Coddington, P. and Macian, R. (2002), "A Study of the Performance of Void Fraction Correlations Used in the Context of Drift-Flux Two-Phase Flow Models," Nuclear Engineering and Design, Vol. 215, pp. 199–216.

Durant, W. B. (2003), "Heat Transfer Measurement of Annular Two-Phase Flow in Horizontal and a Slightly Upward Inclined Tube," M.S. Thesis, Oklahoma State University, Stillwater, OK.

Ghajar, A. J. (2005), "Non-Boiling Heat Transfer in Gas-Liquid Flow in Pipes – a Tutorial," Journal of the Brazilian Society of Mechanical Sciences and Engineering, Vol. XXVII, No. 1, pp. 46-73.

Ghajar, A. J. and Kim, J. (2005), "A Non-Boiling Two-Phase Flow Heat Transfer Correlation for Different Flow Patterns and Pipe Inclination Angles," Proceedings of the 2005 ASME Summer Heat Transfer Conference, July 17-22, San Francisco, CA, Paper No. HT2005-72078.

Ghajar, A. J. and Kim, J. (2006), "Calculation of Local Inside-Wall Convective Heat Transfer Parameters from Measurements of the Local Outside-Wall Temperatures along an Electrically Heated Circular Tube," Heat Transfer Calculations, edited by M. Kutz, McGraw-Hill, New York, pp. 23.3–23.27.

Ghajar, A. J., Kim, J., Durant, W. B., and Trimble, S.A. (2004a), "An Experimental Study of Heat Transfer in Annular Two-Phase Flow in a Horizontal and Slightly Upward Inclined Tube," HEFAT2004: Proc. 3rd International Conference on Heat Transfer, Fluid Mechanics and Thermodynamics, June 21-24, Cape Town, South Africa, Paper No. GA1.

Ghajar, A. J., Kim, J., Malhotra, K., and Trimble, S.A. (2004b), "Systematic Heat Transfer Measurements for Air-Water Two-Phase Flow in a Horizontal and Slightly Upward Inclined Pipe," ENCIT2004: Proc. of the 10th Brazilian Congress of Thermal Sciences and Engineering, Nov. 29-Dec. 3, Rio de Janeiro, Brazil, Paper No. CIT04-0471.

Ghajar, A. J., Kim, J., and Tang, C. (2006), "Two-Phase Flow Heat Transfer Measurements and Correlation for the Entire Flow Map in Horizontal Pipes," Proceedings of the 13th International Heat Transfer Conference, Aug. 13-18, Sydney, Australia.

Ghajar, A. J., Malhotra, K., Kim, J., and Trimble, S. A. (2004c), "Heat Transfer Measurements and Correlations for Air-Water Two-Phase Slug Flow in a Horizontal Pipe," HT-FED2004: Proc. of 2004 ASME Heat Transfer/Fluids Engineering Summer Conference, July 11-15, Charlotte, North Carolina, Paper No. HT-FED2004-56614.

Ghajar, A. J. and Tang, C. C. (2007), "Heat Transfer Measurements, Flow Pattern Maps and Flow Visualization for Non-Boiling Two-Phase Flow in Horizontal and Slightly Inclined Pipe," Heat Transfer Engineering, Vol. 28, No. 6, pp. 525-540.

Hetsroni, G., Hu, B. G., Yi, B. G., Mosyak, A., Yarin, L. P., and Ziskind, G. (1998), "Heat Transfer in Intermittent Air-Water Flow–Part II: Upward Inclined Tube," Int. J. Multiphase Flow, Vol. 24, No. 2, pp. 188–212.

Kim, D. and Ghajar, A. J. (2002), "Heat Transfer Measurements and Correlations for Air-Water Flow of Different Flow Patterns in a Horizontal Pipe," Experimental Thermal and Fluid Science, Vol. 25, pp. 659–676.

Kim D., Ghajar A. J., and Dougherty R. L. (2000), "Robust Heat Transfer Correlation for Turbulent Gas-Liquid Flow in Vertical Pipes," J. Thermophysics and Heat Transfer, Vol. 14, No. 4, pp. 574–578.

Kim, D., Ghajar, A. J., Dougherty, R. L., and Ryali, V. K. (1999), "Comparison of 20 Two-Phase Heat Transfer Correlations with Seven Sets of Experimental Data, Including Flow Pattern and Tube Inclination Effects," Heat Transfer Engineering, Vol. 20, No. 1, pp. 15–40.

Kim, J. and Ghajar, A. J. (2006), "A General Heat Transfer Correlation for Non-Boiling Gas-Liquid Flow with Different Flow Patterns in Horizontal Pipes," International Journal of Multiphase Flow, Vol. 32, No. 4, pp. 447–465.

Kline, S. J. and McClintock, F. A. (1953), "Describing Uncertainties in Single-Sample Experiments," Mech. Engr., Vol. 1, pp. 3–8.

Lockhart, R. W. and Martinelli, R. C. (1949), "Proposed Correlation of Data for Isothermal Two-Phase, Two Component Flow in Pipes," Chemical Engineering Progress, Vol. 45, No. 1, pp. 39–48.

Rouhani, S. Z. and Axelsson, E. (1970), "Calculation of Void Volume Fraction in the Subcooled and Quality Boiling Regions," International Journal of Heat Mass Transfer, Vol. 13, pp. 383–393.

Sieder, E.N. and Tate, G.E. (1936), "Heat Transfer and Pressure Drop of Liquids in Tubes," Industrial & Engineering Chemistry,Vol. 28, No. 12, pp. 1429–1435.

Spedding, P. L. and Chen, J. J. J. (1984), "Holdup in Two Phase Flow," International Journal of Multiphase Flow, Vol. 10, No. 3, pp. 307–339.

Taitel, Y and Dukler, A. E. (1976), "Model for Predicting Flow Regime Transitions in Horizontal and Near Horizontal Gas-Liquid Flow," AIChE Journal, Vol. 22, No. 1, pp. 47–55.

Trimble, S. A., Kim, J., and Ghajar, A. J. (2002), "Experimental Heat Transfer Comparison in Air-Water Slug Flow in Slightly Upward Inclined Tube," In Proc. 12th International Heat Transfer Conference, Heat Transfer 2002, pp. 569–574, Elsevier.

Woldesemayat, M. A. and Ghajar, A. J. (2007), "Comparison of Void Fraction Correlations for Different Flow Patterns in Horizontal and Upward Inclined Pipes," International Journal of Multiphase Flow, Vol. 33, pp. 347-370.